Conformational Changes in Actinin-type Actin Binding Domains: Probing Actin-induced Structural Dynamics in Dystrophin and Utrophin using EPR Spectroscopy.

A THESIS
SUBMITTED TO THE FACULTY OF
UNIVERSITY OF MINNESOTA
BY

Jonathan Crain

IN PARTIAL FULFILLMENT OF THE REQUIREMENTS
FOR THE DEGREE OF MASTER OF SCIENCE

Dr. David D. Thomas

December 2014

Acknowledgements

There are many people without which this thesis would not exist. First and foremost, Dave Thomas offered me space in his lab when there was none elsewhere, and kept me on even when I was struggling.

There are almost too many members of the Thomas Lab to thank. Octavian Cornea and Sarah Blakely Anderson have provided tremendous technical, scientific, and personal support to the entire Thomas Lab, myself included. Ava Yun Lin established the foundations of this project, and helped to bring me into the lab even as she was busy graduating into the M.D. portion of her MD/Ph.D. program. Ewa Prochniewicz and Piyali Guhathakurta have been generous with their time, teaching me how to work with actin, lending me reagents, and answering my questions.

Special credit is due to Gage Matthews, a former Thomas Lab EPR jock, who was instrumental in generating and analyzing the data presented within this thesis. Mike Fealey, who recently joined the Thomas Lab, has not only helped to continue our work on dystrophin but has also helped me navigate the process of a writing a thesis. To say that Ben Binder has provided useful discussion with regard would be an understatement. Special thanks are also owed to Ben for adding spin labels to existing molecular models, which I subsequently using to create better figures. Beyond those named here, there is probably not a single member of the Thomas Lab who has not helped me in some way.

This work would not have been possible without the Roberto Dominguez and David Kast at the University of Pennsylvania. Spurred by previous work from Ava Yun Lin and the Thomas Lab, they generated, expressed, and labeled utrophin and dystrophin constructs for the experiments presented in this thesis.

I would also like to thank my committee members, both past and present, for valuable discussions and advice. This includes Jim Ervasti, Ian Armitage, Gianluigi Veglia,

Lincoln Potter, and Dawn Lowe. I'd also like to thank Kathleen Conklin, who went above and beyond her duty as Director of Graduate Studies.

This worked was funded by 5R01AR063007-03 from the National Institute of Arthritis and Musculoskeletal and Skin Diseases.

Dedication

The completion of this thesis is dedicated to memory of my grandfather.

Abstract

The underlying cause of Duchenne and Becker muscular dystrophies is a lack of functional dystrophin, a large multidomain protein. Dystrophin is normally expressed in muscle, where it links the extracellular matrix to the cortical actin cytoskeleton via a complex of associated proteins. Dystrophin, and its autosomal homologue utrophin, connect with the actin cytoskeleton through two F-actin binding domains, including an N-terminal "actinin-type" actin binding domain (ABD).

In addition to dystrophin and utrophin, actinin-type ABDs are found in a large number of proteins. Nonetheless, the actin binding mechanism remains poorly understood: x-ray crystallography and electron microscopy have produced conflicting models. Electron paramagnetic resonance (EPR) spectroscopy, especially double electron-electron resonance (DEER), can be used to distinguish between these models or to build new models. In this thesis, I present data from DEER experiments which suggest that actinin-type ABDs of dystrophin and utrophin adopt unexpected conformations in solution.

Table of Contents

List of Tables

List of Figures

Chapter 1 | Dystrophin, Utrophin, and Duchenne/Becker Muscular Dystrophy

1.1 | Dystrophin is a large structural protein required for muscle cell integrity.

Dystrophin is a large (427 kDa) multidomain protein expressed in muscle, where it localizes to costameres (*1*). At its N-terminus, the dystrophin protein contains the first of two actin binding domains (DysABD1) (Fig. 1**A**). DysABD1 is followed by a rod-like region of 24 spectrin type repeats, within which are four hinge regions. Spectrin repeats 11 through 17 constitute the second actin binding domain (DysABD2). Repeats within the rod domain also allow dystrophin to bind to microtubules (*2*). The rod is followed by a cysteine-rich domain and a C-terminal domain, which bind to β-dystroglycan and α-dystrobrevin, respectively (*1, 3, 4*).

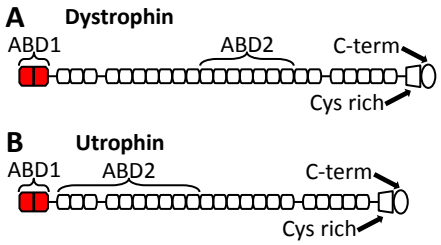

Fig. 1. Dystrophin and Utrophin. (**A**) The N-terminal ABD1 of dystrophin is made up of two CH domains, connected to the 24 spectrin type repeat (STR) rod domain, followed by the Cys-rich and C-terminal domains. STRs 11-17 act as an additional ABD. (**B**) Utrophin is similar; 2 STRs are deleted and the ABD2 is contiguous with the ABD1. (*1*)

β-dystroglycan and α-dystrobrevin are members of the dystrophin-glycoprotein complex, which is composed of sarcoplasmic, transmembrane, and extracellular proteins (*3*). The dystrophin-glycoprotein complex binds to intermediate filaments in the extracellular matrix. Dystrophin thus forms a physical link at costameres between the extracellular matrix and cortical actin, helping to stabilize the sarcolemma during contraction (*5*).

Stabilization of the sarcolemma by dystrophin is crucial for the maintenance of muscle cell integrity. Duchenne muscular dystrophy (DMD), a severe X-linked disorder,

results from mutations which caused either a loss of function in dystrophin or a reduction of dystrophin expression (*6, 7*). Although the precise molecular mechanisms are uncertain, in the absence of dystrophin the sarcolemma becomes vulnerable to damage during muscle contraction. Intracellular calcium is increased, and muscle undergoes continuous degeneration and regeneration, with increasing fibrosis (*8-12*). In humans, muscle weakness is typically observed around age 5, leading to diagnosis (*13*). Without the use of glucocorticoid corticosteroids, affected boys are wheelchair-bound by their teenage years, and die during their late teens or early twenties. Less severe mutations result in expression of a partially functional dystrophin, leading to Becker muscular dystrophy (BMD). The severity of the BMD phenotype is variable, but is generally similar to DMD, although often more mild (*13, 14*).

The actin binding property of dystrophin is fundamentally necessary to its function. An N-terminally truncated dystrophin isoform lacking DysABD1 only partially rescued the mdx mouse model of DMD, while *in trans* co-expression of N-terminal and C-terminal dystrophin constructs failed to rescue both the *mdx* and *dko* mouse models of DMD (*15, 16*). These results demonstrate that each dystrophin molecule must directly interact with both cortical F-actin and the dystroglycan complex, making DysABD1 especially important for dystrophin function.

1.2 | Utrophin is an autosomal homologue of dystrophin.

Utrophin is an autosomal homologue of dystrophin which is expressed even in DMD/BMD patients (*17-19*). Expressed ubiquitously during embryonic development, utrophin then becomes restricted to the myotendinous and neuromuscular junctions in

adults. The 394 kDa utrophin protein is substantially similar to dystrophin: like dystrophin, utrophin contains an N-terminal ABD (UtrABD1), followed by a rod region composed of spectrin repeats, as well as cysteine-rich and C-terminal domains which interact with the dystroglycan complex (Fig. 1**B**) (*1, 4*).

As in dystrophin, utrophin also has second actin binding region within the rod domain, although in utrophin the ABD2 is composed of repeats 1-10. Unlike dystrophin, utrophin does not recruit neuronal nitric oxide synthase to the sarcolemma, and does not bind microtubules (*20, 21*). Utrophin is also slightly smaller, lacking two spectrin repeats as compared to dystrophin (*1*).

The similarities between dystrophin and utrophin appear to be greater than their differences, since overexpression of utrophin rescues the *mdx* mouse (*22*). Utrophin-based gene therapy strategies for DMD/BMD are therefore of major interest as an alternative to dystrophin-based strategies, especially following the failure of a dystrophin-based gene therapy trial due to an immune response targeting dystrophin (*23-25*).

1.3 | Understanding dystrophin and utrophin structure to design better therapies.

Pharmacological and non-pharmacological interventions have begun to change the natural history of DMD, leading to longer lifespans and improved quality of life (*26*). Nonetheless, treatment options remain limited, with pharmacological options restricted to glucocorticoid corticosteroids (i.e., prednisone, prednisolone, and deflazacort). Continuous glucocorticoid corticosteroid treatment merely delays disease progression, and is accompanied by strong side effects (*27-29*). DMD therefore remains a serious

disease for which new treatment options are continually sought (*25, 30*).

Since DMD and BMD are genetic diseases arising from mutations within a single gene, the most direct approach would be to complement the native gene with one encoding a functional dystrophin. Major efforts have therefore been dedicated to the development of gene therapy for DMD. To avoid problems arising from an immune response to dystrophin, utrophin has also been considered as a dystrophin replacement (*25*).

Adeno-associated viral vectors are commonly favored, but have a limited genomic capacity of ~5 kB. Since the dystrophin mRNA is ~14 kB, this has necessitated the creation of "micro" dystrophin and utrophin constructs (*31*). Such constructs draw inspiration from BMD patients who display relatively minor symptoms despite especially large deletions in the gene encoding dystrophin (*32*). Although gene therapy has proven difficult to translate into an approved clinical treatment, animal models have provided a proof of concept (*22-24, 33*).

Designing miniaturized dystrophin or utrophin constructs for use in gene therapy requires compromise with regard to gene size versus protein function. For instance, a dystrophin construct lacking the ABD2 will have a reduced affinity for actin, which may in turn reduce its therapeutic potential. With improved structural understanding of dystrophin and utrophin, it may be possible to engineer improved constructs which retain a greater proportion of their normal functional. With respect to actin binding, naturally occurring mutations which increase actin binding affinity have been observed in the ABD of α-actinin (which is homologous to the ABD1 in dystrophin) (*34-36*). In a dystrophin

construct lacking the ABD2, such a mutation might prove beneficial rather than harmful. That is, if the actin binding mechanism of the ABD1 were understood, then it might be possible to tune the binding affinity of the dystrophin/utrophin ABD1 and improve the overall function of a micro dystrophin/utrophin construct.

Chapter 2 | Dystrophin and Utrophin Actin Binding Domain 1

2.1 | Introduction

The N-terminal actin binding domains of dystrophin and utrophin (DysABD1 and UtrABD1), belong to the actinin-type family of actin binding domains. (*37-39*). Actinin-type ABDs are found in a wide variety of F-actin binding proteins, including α-actinin, β-spectrin, fimbrin, filamin, and plectin, in addition to utrophin and dystrophin. Isolated DysABD1 and UtrABD1 constructs bind F-actin with micromolar affinity; in combination with their respective ABD2s, they allow dystrophin and utrophin to bind to F-actin with sub-micromolar affinity (*40-44*).

Fig. 2. X-ray Crystal Structure of DysABD1. DysABD1 crystallized as an antiparallel dimer, suggesting either an open conformation (D) or a closed conformation (E) similar that of α-actinin (F). UtrABD1 (not shown) crystallized as a dimer similar to that of DysABD1 (*45-47*).

Crystal structures have been determined for several actinin-type ABDs, including utrophin and dystrophin (*45, 46*). These structures show that actinin-type ABDs are themselves composed of a pair of tandem calponin homology domains (CH1 and CH2). Each CH domain is composed of a "sandwich" of 4 major α-helices connected by more variable minor α-helices and loops, with CH1 and CH2 connected by an α-helical linker. Despite the similarity between CH1 and CH2, CH1 is generally more similar to CH1 from other actinin-type ABDs than to CH2 from the same domain, and vice versa (*39*).

The crystal structures of DysABD1 and UtrABD1 differ significantly from the

crystal structures of other actinin-type ABDs. Whereas ABDs from α-actinin, plectin, and fimbrin crystallized as compact monomers in which the CH domains are folded back upon each other, dystrophin and utrophin have crystallized as dimers in which each protomer adopts a more extended conformation (Fig. 2**A**) (*47-50*). However, in these dimeric structures, CH1 and CH2 from opposite members of the dimer are closely apposed, resulting in a compact structure similar to that from α-actinin crystals via domain swapping (Fig. 2**B, C**).

The unusual dimeric crystal forms of UtrABD1 and DysABD1, combined with an inability to crystallize F-actin, created uncertainty as to how DysABD1 and UtrABD1 might bind to actin. Subsequently, Galkin, et al. (*51*) published a model of the UtrABD1 bound to F-actin reconstructed from electron micrographs. In this "open EM" model, UtrABD1 occupies an open conformation similar to, but more extended than, the protomer within the x-ray crystal dimer. However, Sutherland-Smith, et al. (*52*), also using electron microscopy, subsequently published models for both UtrABD1 and DysABD1 bound to actin in a closed conformation, similar to that seen by domain swapping within the x-ray crystal structures ("closed EM" models). Therefore, electron microscopy has been unable to distinguish between the possible closed an open binding modes of DysABD1 and UtrABD1.

The distance between a given point on CH1 and a given point on CH2 is a distinguishing characteristic of each model; a short distance is predicted by the closed EM models, while the distance between the same points in the x-ray crystal protomer or in the open EM model of utrophin is greater. Lin, et al. (*53*) took advantage of this

property to determine the conformation of UtrABD1 free in solution and bound to F-actin using double electron-electron resonance (DEER).

DEER is a pulsed electron paramagnetic resonance (EPR) technique capable of determining both distance distribution between two spin labels, if the distances are on the order of 2-8 nm (Fig. 3). Site directed spin labeling allows the placement of the thiol-reactive maleimide spin label (MSL) at selected residues within a protein which have been mutated to cysteine. Native cysteine residues, if any, are mutated to alanine or serine (*54-57*).

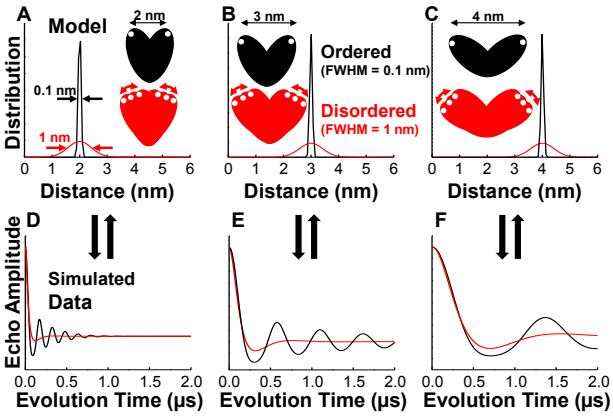

Fig. 3. DEER is sensitive to distance and disorder. A-C: Two single Gaussian distributions (as of a doubly spin-labeled molecule in solution) which differ in amount of disorder were simulated with centers at 2 nm (**A**), 3 nm (**B**), or 4 nm (**C**). The simulated DEER waveforms for these populations are shown in **D-F**, respectively. In all cases, the waveforms are sufficiently different to distinguish between both distance center and disorder.

By mutating a single residue within each CH domain of UtrABD1 to cysteine and labeling with MSL, Lin, et al. (*53*) were able determine the distance between CH domains via DEER. In the absence of actin, UtrABD1 was found to exist in equilibrium between two states: one which agreed well with the distance expected of the crystal protomer, and a somewhat more extended state. Moreover, upon the addition of F-actin, the distance between CH1 and CH2 increased and was most consistent with the open EM model of Galkin, et al. (*51*). Importantly, no evidence of a short distance suggestive of a closed conformation was observed.

In order extend and confirm the conclusions reached by Lin, et al.(*53*), DysABD1 and UtrABD1 were both labeled with MSL at novel sites, one per CH domain. DEER experiments were then carried out either in the absence of actin or in the presence of up to a four-fold molar excess of F-actin, and the distance distributions determined from the DEER waveforms.

2.2 | Materials & Methods

2.2.1 | Protein Purification and Spin Labeling

Plasmids encoding murine UtrABD1 (residues 1-261, UniProt O08614) and murine DysABD1 (residues 1-246, UniProt P11531) were provided to Roberto Dominguez and David Kast at the University of Pennsylvania. DEER constructs were then generated, expressed, and labeled at the University of Pennsylvania.

Constructs were generated as previously (*58*). UtrABD1 and DysABD1 were subcloned into pTYB11 (New England BioLabs), resulting in an N-terminal fusion of a chitin affinity tag and an intein domain. UtrABD1 constructs in which S54, T220, or both S54 and T220 were mutated to cysteine (S54C, T220C, S54C:T220C) were generated. To improve the stability of DysABD1, residues 2-8 were deleted and C9 was mutated to aspartic acid. DysABD1 constructs were then generated either by mutating D38 to cysteine and C205 to serine (for singly-labeled controls) or by only mutating D38 to cysteine (D38C:C205). All mutagenesis was carried out using a QuikChange II XL site-directed mutagenesis kit (Strategene).

All constructs were expressed in *Escherichia coli* BL21(DE3) cells. As previously described, cells were re-suspended and lysed using a microfluidizer and the construct

purified on a chitin affinity column. The chitin tag was removed by inducing self-cleavage of the intein, after which the constructs were further purified using a Superdex-200 size exclusion column (GE Healthcare).

UtrABD1 and DysABD1 constructs were labeled with MSL [N-(1-Oxyl-2,2,6,6-tetramethyl-4-piperidinyl)maleimide]. Labeled samples were exchanged into 50 mM Tris pH 7.5, 100 mM NaCl. Complete labeling was determined by mass spectrometry. Labeled proteins were then shipped on ice to the University of Minnesota, where samples for DEER were made immediately upon receipt.

2.2.2 | Preparation of F-actin

Actin was prepared from acetone powder derived from rabbit skeletal muscle as described previously (*59*). Acetone powder was incubated for 30 minutes on ice in water pre-chilled to 4°C. The mixture was then filtered, and 30 mM KCl was added to the filtrate. Following 60 minutes incubation at room temperature the filtrate (containing the polymerized actin) was centrifuged either in a Beckman TLA100.3 rotor for 30 minutes at 80,000 rpm at 4°C (for small volumes) or in a Beckman Type Ti70.1 rotor for 60 minutes at 50,000 rpm at 4°C (for larger volumes). The supernatant was discarded, and the pellet (containing the polymerized actin) was washed and then re-suspended in G-buffer (5 mM Tris pH 7.5, 0.5 mM ATP, 0.2 mM $CaCl_2$.) The G-actin was then clarified by centrifugation in a Beckman TLA100.3 rotor at 70,000 rpm for 10 minutes at 4°C. The amount of G-actin recovered was then determined by UV/Vis spectrophotometry based on an extinction coefficient at ε_{290}=0.63 ml mg^{-1} cm^{-1}. The actin was then re-polymerized by adding 2 mM $MgCl_2$ and incubating at room temperature for 30 minutes.

The F-actin was then pelleted by centrifugation in a Beckman TLA100.3 rotor at 80,000 rpm for 30 minutes at 4°C, and the pelleted F-actin re-suspended to the desired concentration in F-buffer (25 mM Tris pH 8.0, 100 mM NaCl, 0.5 mM ATP, 2 mM $MgCl_2$, 1 mM DTT).

2.2.3 | DEER

Sample Preparation: UtrABD1 S54C.MSL:T220C.MSL, UtrABD1 S54C.MSL, UtrABD1 T220C.MSL, DysABD1 D38C.MSL:C205.MSL, or DysABD1 D38C.MSL was mixed to 80 μM with either a 0.5-fold, two-fold, or four-fold molar excess of F-actin in 25 mM Tris pH 8.0, 100 mM NaCl, 2 mM $MgCl_2$, with 10% (v/v) glycerol. After mixing, samples were allowed to incubate on ice for 30 minutes. 15 μL samples were then flash frozen in liquid nitrogen, and stored at -80°C. Actin-free samples were prepared similarly, except that additional F-buffer was used to maintain the correct volume.

Data Acquisition and Analysis: DEER was performed on a Bruker EleXys E580 Q-band instrument cooled to 65K. DEER waveforms were analyzed using DEER Analysis 2008, an open-source software package for Matlab (*60*).

Table 1. Labeling sites used and predicted Cα-Cα distances in nm.

	Closed EM (*52*)	Closed Crystal[1] (*45, 46*)	Open Crystal[2] (*45, 46*)	Open EM (*51*)
UtrABD1 S54C T220C	2.4	2.4	6.4	7.7
DysABD1 D38C C205	2.4	2.2	6.8	-

UtrABD1 and DysABD1 were labeled with MSL at the named residues. Distances between residues are measured from Cα to Cα in nm.
[1]Measured from protomer A to protomer B within the crystal dimer.
[2]Measured within a single protomer.

2.3 | Results

2.3.1 | Utrophin ABD1

UtrABD1 was labeled with MSL at S54C and T220C. For this set of labeling sites, the closed EM model from Sutherland-Smith, et al. (*52*) predicts a Cα-Cα distance of 2.4 nm, in accordance with the distance between opposite members of the dimer observed by x-ray crystallography (**Table 1**) (*46*). The x-ray protomer predicts a larger Cα-Cα distance of 6.4 nm, while the open EM model from Galkin, et al. (*51*) predicts a distance of 7.7 nm. The closed and open models should therefore be distinguishable by DEER,

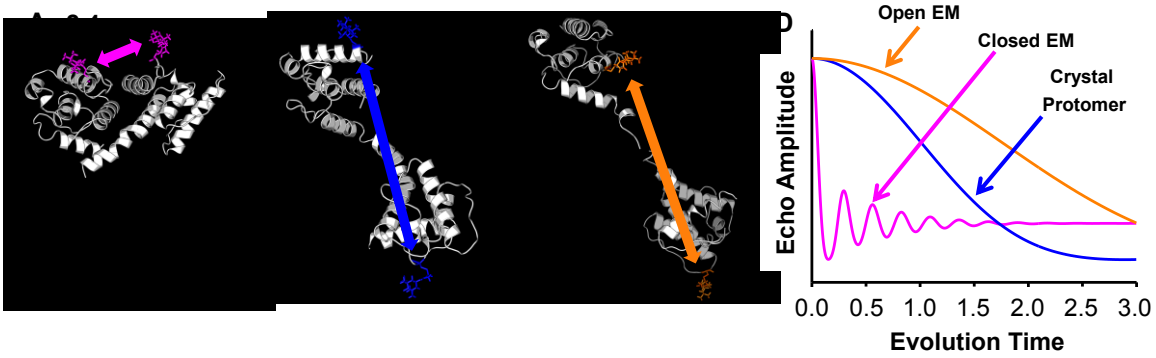

Fig. 4. Simulated UtrABD1 DEER waveforms. Distances between residues 54 and 220 of UtrABD1 as measured from Cα-Cα for the closed EM structure (**A**), the x-ray crystal protomer (**B**), or the open EM structure (**C**), and simulated DEER waveforms (**D**). The difference between a short distance/closed structure and a long distance/open structure is readily apparent. (*46, 51, 52*)

based on simulated spectra for each of these distances (**Fig. 4**).

Initial analysis of the DEER waveforms showed that, in the absence of actin, the distance between the labels at S54C and T220C fit best to a single Gaussian distribution centered at 3.7 nm (Fig. 5**A**). As F-actin was added in increasing amounts, a two Gaussian model fit best (Fig. 5**B-H**). At 0.5 mol actin/mol UtrABD1, the Gaussians were

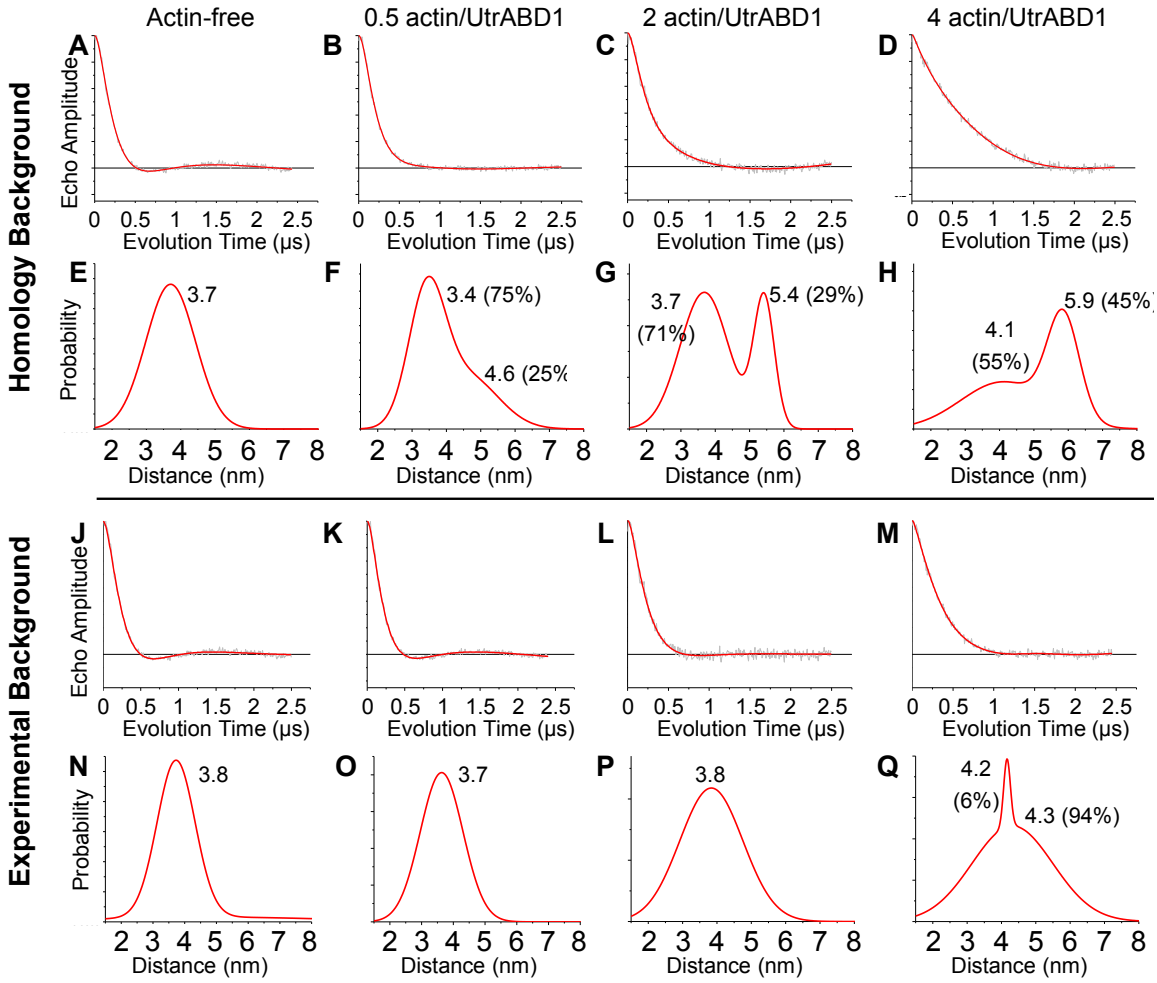

Fig. 5. DEER waveforms for UtrABD1. UtrABD1 was labeled with MSL at residues 54 and 220, and DEER was performed without actin, at 0.5 mol actin/mol UtrABD1, 2 mol actin/mol UtrABD1, or 4 mol actin/mol UtrABD1. The corresponding distance distributions are shown below their respective spectra. Numbers represent the center of the Gaussian represented by the adjacent peak, in nm. **A-H:** Background correction was performed by allowing DEER Analysis 2008 to computationally fit the background with a homogenous model ("Homology Background"). **J-Q:** As in A-H, except that background correction was performed using functions derived from equivalent DEER experiments in which UtrABD1 was labeled at only residue 54 or only at residue 220.

centered at 3.4 nm and 4.6 nm. At 2 mol actin/mol UtrABD1, the two Gaussians were centered at 3.7 nm and 5.4 nm. At 4 mol actin/mol UtrABD1, the two Gaussians were centered at 4.1 nm and 5.9 nm. Notably, as the amount of F-actin added increased, the proportion of the population at the longer distance became more prominent.

Taken together, this data suggested that in the absence of actin UtrABD1 adopts a conformation such that the distance between residues 54 and 220 is 3.7 nm. The data also suggested that the actin-bound UtrABD1 adopts a conformation such that the distance between these two residues is increased, though the long distance and amount of disorder made it difficult to determine the distance precisely.

To improve the fits and eliminate artifacts due to filamentous nature of F-actin, spectra were acquired from UtrABD1 labeled at a single cysteine (either S54C or T220C) mixed with F-actin. When these experimentally derived background spectra were used during the fitting process, a longer distance no longer appeared as F-actin was added. The spectra could largely be fit by a single Gaussian centered at about 3.7 nm, with a slight increase in distance to about 4.3 nm at high concentrations of F-actin (Fig. 5**J-Q**). This suggested that UtrABD1 adopts a relatively closed conformation when free in solution, though somewhat more extended and disordered than suggested by the crystal structure, and that the UtrABD1 rearranges upon binding to F-actin such that the distance between CH1 and CH2 is increased slightly.

2.3.2 | Dystrophin ABD1

DysABD1 was labeled with MSL at D38C and C205. The Cα-Cα distance between these two residues is predicted to be 2.4 nm by the closed EM structure published by Sutherland-Smith, et al. (*52*). Likewise, the Cα-Cα distance between these two residues on opposite monomers within the x-ray crystal dimer is 2.2 nm (*45*). When measured between residues within a single monomer, the crystal predicts a distance of 6.8 nm (**Table 1**). There is no open EM model of DysABD1, the existence of an open EM

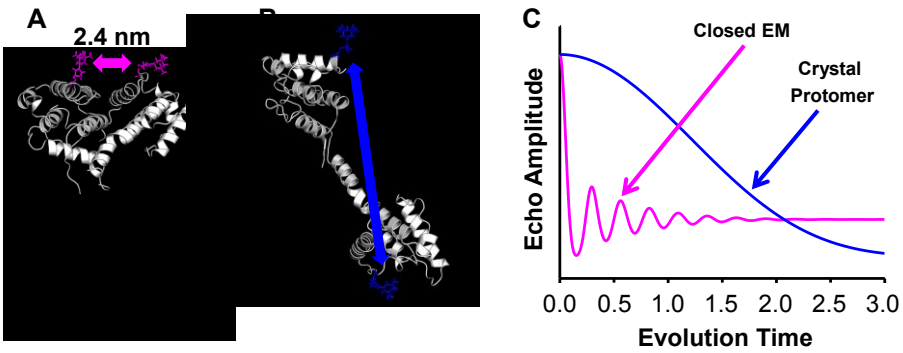

Fig. 6. Simulated DysABD1 DEER waveforms. Distances between residues 38 and 205 of DysABD1 as measured from Cα-Cα for the closed EM structure (**A**) and the x-ray crystal protomer (**B**). Simulated DEER waveforms for these distances (**C**) show that a short distance/closed structure and a long distance/open structure are readily distinguished. (*45, 52*)

structure for UtrABD1 suggests that a similar conformation might be possible for DysABD1: that is, one which is similar to the crystal protomer but somewhat more extended. Importantly, there is a large difference between the distance predicted by closed and open models, so DEER should be able to distinguish between the two (**Fig. 6**).

Initial analysis of the DEER waveforms suggested that, in the absence of actin, the range of conformations adopted by DysABD1 is best fit a 2-Gaussian model with the bulk of the population (65%) centered at 2.5 nm, and a smaller subset at 3.5 nm (Fig. 7**A, E**). As F-actin was added to DysABD1, the observed distance distribution did not change substantially, even at a four-fold excess of actin (Fig. 7**B-D, F-H**).

To improve the reliability of the fits, the DEER waveforms were re-analyzed using data from equivalent DEER experiments in which DysABD1 was labeled only at D38C to improve the background subtraction (Fig. 7**J-Q**). Unlike for UtrABD1, the more

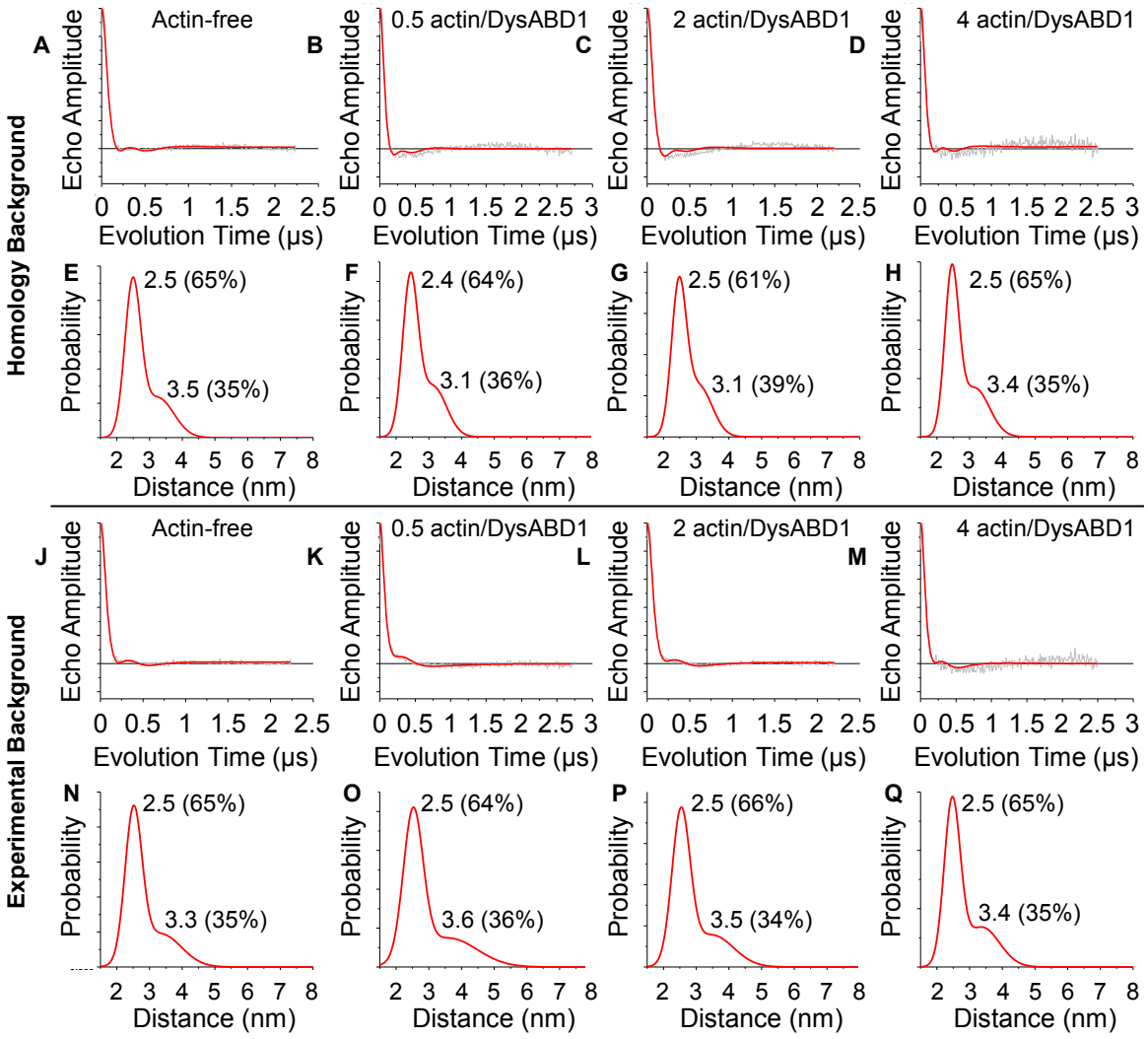

Fig. 7. DEER waveforms for DysABD1. DysABD1 was labeled with MSL at residues 38 and 205, and DEER was performed without actin (**A**), at 0.5 mol actin/mol DysABD1 (**B**), 2 mol actin/mol DysABD1 (**C**), or 4 mol actin/mol DysABD1 (**D**). The corresponding distance distributions (**E-H**) are shown below their respective spectra. Numbers represent the center of the Gaussian represented by the adjacent peak, in nm. **A-H:** background subtraction was performed by allowing DEER Analysis 2008 to computationally fit the background a homogenous model ("Homology Background"). **J-Q:** as in A-H, except that background subtraction was performed using functions derived from equivalent DEER experiments in which DysABD1 was labeled at only residue 38.

rigorous analysis did not substantially change the interpretation of the spectra. Both in the absence of actin and when mixed with F-actin up to a four-fold molar excess, the distance distributions again showed that DysABD1 adopts a conformation which can best be modeled as the sum of two overlapping Gaussians. The first Gaussian, accounting for approximately two thirds of the population, is centered at 2.5 nm and is relatively narrow, while a second broader Gaussian centered at 3.3-3.6 nm accounts for the remaining third of the population.

Notably, the 2.5 nm distance which represents the bulk of the population, agrees reasonably well with the 2.4 nm predicted by the closed EM model. This suggests that the bulk of the population adopts a closed conformation even while bound to actin, whereas a subset of the population occupies a more extended conformation.

2.4 | Discussion

2.4.1 | The utrophin ABD1 may adopt a novel conformation in solution.

Initial analysis of the DEER waveforms suggested that UtrABD1 adopts a relatively closed conformation while free in solution, albeit not as compact as predicted by the closed EM models. The same analysis suggested that when bound to actin, UtrABD1 adopts a more extended conformation (Fig. 5**A-H**).

However, a more rigorous analysis using experimentally derived spectra for background subtraction suggested that there is actually little change in the conformation of UtrABD1 upon the addition of F-actin (Fig. 5**J-Q**). Instead, UtrABD1 appears to remain in a conformation which is neither as compact as predicted by the closed EM model or the domain swapped x-ray crystal, nor as extended as predicted by the open EM

model. This suggests that UtrABD1, when in solution, occupies a conformation different from what had previously been predicted by either x-ray crystallography or electron microscopy.

In the previous work by Lin, et al. (*53*), UtrABD1 was labeled with MSL at V136C and L222C. Lin and colleagues determined that, when free in solution, UtrABD1 exists in equilibrium between two states, one of which agrees with the x-ray crystal monomer. UtrABD1 was also found to occupy a second more extended conformation. By adding F-actin, Lin et al. (*53*) then determined that the UtrABD1 binds to actin filaments in an extended conformation corresponding to the open EM model. These conclusions are in strong contrast to those suggested by Fig. 5.

The discrepancy may be explained in several ways. In the simplest case, we might reject the data presented in Fig. 5 in favor of the data and conclusions presented by Lin, et al (*53*). Of the two sets of experiments, theirs was the better controlled: Lin, et al. present supplemental data showing that neither mutagenesis of their labeling sites to cysteine, nor labeling with MSL, altered actin binding function based on an actin co-sedimentation assay. Circular dichroism was also used to show that site directed spin labeling did not disturb UtrABD1 secondary structure. Equivalent controls have not yet been carried out for UtrABD1 labeled at S54C/T220C. It may therefore be best to consider the data presented in this thesis as preliminary data, and to weight the conclusions of Lin, et al. (*53*) more heavily.

However, if we assume that site directed spin labeling at S54C and T220C disturbed neither the structure nor function of the UtrABD1, then other explanations

should be considered. The choice of labeling sites is especially important. Lin, et al. (*53*) chose to label at V136C and L222C, since the distance between these residues predicted by each model produced significantly different simulated DEER waveforms, and since each predicted distance was well within the range detectable by either DEER or CW-EPR. However, the choice of V136C places a label close the interface between CH domains in the closed model. Although it is possible to model MSL into the crystal structure of UtrABD1 at V136C without producing steric clashes, in solution the spin label may adopt a conformation which would favor an opening of the UtrABD1.

Based on this concern, Roberto Dominguez and colleagues designed the S54C/T220C labeling sites. This pair of labeling sites places the spin labels on the exterior of the protein, based on both closed and open models. However, the Cα-Cα distance between residues 54 and 220 is 6.4 nm in x-ray crystal protomer, and 7.7 nm in the open EM model. Although these distances are within the theoretical detection limits of DEER, they lay outside the range of what can be reliably detected in difficult samples – such as those containing a high concentration of F-actin. In such samples, the practical upper limit for detection by DEER becomes ~5 nm (*56*). Additionally, the distance between radicals on the actual spin labels may be even greater, depending on the conformation adopted by the labels relative to UtrABD1.

Thus, we have data from two different sets of labeling sites, each of which is imperfect. The sites chosen by Lin, et al. (*53*) may favor the detection of an open conformation, whereas S54C/T220C may fail to accurately detect an open conformation. In order to resolve the discrepancy between these two datasets, it may therefore be

necessary to design new labeling sites. These sites should be within the dynamic range of DEER for actin-bound samples as per Lin, et al. (*53*), but should also be designed using tools such as molecular dynamics simulations to avoid sites where the spin label itself might favor a conformational change in the larger protein construct.

Alternatively, these datasets may not truly be in conflict. By performing rigid body rotations about the residue 149/150 peptide bond, Lin, et al. (*53*) computationally generated a set of at least 21 models of UtrABD1 which satisfied the constraint of a 4.8 nm distance between V136C/L222C, as measured by DEER in the presence of saturating F-actin. Comparing these models visually, by holding one CH domain fixed in the space, it can be seen that the other CH domain rotates about the axis of the UtrABD1 with regard to the first.

Therefore, an opening of the UtrABD1 might be accompanied by a rotation of the CH domains relative to one another. This rotation might either enhance or mitigate an increase in distance due to the larger scale opening of the UtrABD1. In this way, we might see an increase in distance between V136C and L222C upon binding to actin (as measured by Lin, et al.), but little change in the distance between S54C and T220C (as seen in Fig. 5). Conversely, a modest opening of the UtrABD1 accompanied by a rotation of the CH domains relative to one another could also produce this pattern. Orientation information derived from continuous wave EPR will be necessary in order to resolve ambiguity introduced by the possibility of the rotation of the CH domains (*61*).

In either case, UtrABD1 likely occupies a novel conformation seen in neither the x-ray crystal nor modeled based on electron microscopy, both when free in solution and

bound to actin. Such a conformation might nonetheless be substantially similar to those modeled previously, but would incorporate a rotation of the CH domains relative to one another as compared to either the x-ray crystal or one of the EM models.

2.4.2 | Does the dystrophin ABD1 bind actin in a closed conformation?

DysABD1 appears to exist in equilibrium between two conformations. The bulk of the population (~65%) occupies a conformation such that the distance between spin labels at D38C and C205 is 2.5 nm, in close agreement with the 2.4 nm predicted by the closed EM structure (Fig. 7) (*52*). The remaining third of the population occupies a somewhat more extended and disordered conformation, with an average distance between labels at D38C/C205 of ~3.5 nm. Unlike UtrABD1, interpretation of the DEER waveforms did not change significantly depending on the method of background subtraction. Notably, the spectra did not change significantly even with the addition of a four-fold molar excess of F-actin (Fig. 7**J, M**).

As with UtrABD1, several caveats apply. The requisite controls have not been carried out, and therefore this data must be considered preliminary. In order to determine that site direct spin labeling did not disturb the function of DysABD1, actin co-sedimentation experiments must still be carried out. In addition, circular dichroism measurements also need to be made, in order to ensure labeling did not perturb the secondary structure of DysABD1.

Interpretation of the data with respect to the actin-bound conformation of DysABD1 is especially difficult. The lack of an increase in the distance measured by DEER as F-actin was added in increasing amounts may indicate that DysABD1 does not

change conformation upon binding to actin. However, in the absence of co-sedimentation data, it may be that spin labeling is preventing DysABD1 from binding to actin. If DysABD1 adopts a closed conformation in solution, but is being prevented from binding to actin by the spin labels, then we would continue to detect a closed conformation even as actin is added to the sample.

The significance of the 2-Gaussian distribution must similarly be interpreted with caution, especially since the 3.5 nm distance is not predicted by any previous model of DysABD1. Although DysABD1 may be interconverting between two primary conformations, it is also possible that the spin label at either residue 38 or 205 is not isotropically sampling all possible angles with respect to DysABD1. In the latter case, the detection of multiple distances might reflect the conformational selection of the spin label. Molecular dynamics simulations would be useful in distinguishing between these two possibilities.

2.4.3 | Concluding Thoughts

Although further controls are necessary, it is likely that UtrABD1 binds to actin in a conformation not previously modeled. Given the homology between the two domains, the same may apply to DysABD1. In order to build accurate models of UtrABD1 and DysABD1, a number of techniques yielding complementary structural data should be combined.

By designing novel labeling sites, further DEER experiments can provide additional distance information. Similar information could also be derived from fluorescence resonance energy transfer (FRET) experiments using fluorescently labeled

UtrABD1 and DysABD1 (*62, 63*). FRET provides the additional advantage of working in solution at physiological temperatures, as opposed to the cryogenic temperatures required for DEER, and at lower protein concentrations. By placing fluorescent probes at the same labeling sites, FRET can therefore be used to corroborate measurements made by DEER.

With respect to the actin-bound state, conventional EPR can provide information about the angle of a given spin labeled site with regard to the filament (*61*). Finger printing experiments, such as hydrogen/deuterium exchange or hydroxyl radical foot printing coupled to mass spectrometry, can provide information about the solvent accessibility of either the protein backbone or side chains, and can suggest residues likely to interact with F-actin (*64, 65*). Nuclear magnetic resonance (NMR) techniques would be difficult to apply to the actin-bound ABD1s, but could be used to study UtrABD1 and DysABD1 free in solution. Additionally, certain NMR techniques may be able to provide spare structural information about the actin-bound ABD1 (*66-69*).

With enough such information to act as constraints, it will be possible to computationally model UtrABD1 and DysABD1. Especially if done for both the free and actin-bound states, such models might prove useful in engineering improved ABD1s for use in gene therapy.

Bibliography

1. Ervasti, J. M. (2007) Dystrophin, its interactions with other proteins, and implications for muscular dystrophy, *Biochim Biophys Acta 1772*, 108-117.
2. Prins, K. W., Humston, J. L., Mehta, A., Tate, V., Ralston, E., and Ervasti, J. M. (2009) Dystrophin is a microtubule-associated protein, *The Journal of cell biology 186*, 363-369.
3. Davies, K. E., and Nowak, K. J. (2006) Molecular mechanisms of muscular dystrophies: old and new players, *Nat Rev Mol Cell Biol 7*, 762-773.
4. Broderick, M. J., and Winder, S. J. (2005) Spectrin, alpha-actinin, and dystrophin, *Adv Protein Chem 70*, 203-246.
5. Pasternak, C., Wong, S., and Elson, E. L. (1995) Mechanical function of dystrophin in muscle cells, *The Journal of cell biology 128*, 355-361.
6. Bonilla, E., Samitt, C. E., Miranda, A. F., Hays, A. P., Salviati, G., DiMauro, S., Kunkel, L. M., Hoffman, E. P., and Rowland, L. P. (1988) Duchenne muscular dystrophy: deficiency of dystrophin at the muscle cell surface, *Cell 54*, 447-452.
7. Henderson, D. M., Lee, A., and Ervasti, J. M. (2010) Disease-causing missense mutations in actin binding domain 1 of dystrophin induce thermodynamic instability and protein aggregation, *Proc Natl Acad Sci U S A 107*, 9632-9637.
8. Deconinck, N., and Dan, B. (2007) Pathophysiology of duchenne muscular dystrophy: current hypotheses, *Pediatr Neurol 36*, 1-7.
9. Cullen, M. J., and Jaros, E. (1988) Ultrastructure of the skeletal muscle in the X chromosome-linked dystrophic (mdx) mouse. Comparison with Duchenne muscular dystrophy, *Acta Neuropathol 77*, 69-81.
10. Shin, J., Tajrishi, M. M., Ogura, Y., and Kumar, A. (2013) Wasting mechanisms in muscular dystrophy, *Int J Biochem Cell Biol 45*, 2266-2279.
11. Petrof, B. J. (1998) The molecular basis of activity-induced muscle injury in Duchenne muscular dystrophy, *Mol Cell Biochem 179*, 111-123.
12. Petrof, B. J., Shrager, J. B., Stedman, H. H., Kelly, A. M., and Sweeney, H. L. (1993) Dystrophin protects the sarcolemma from stresses developed during muscle contraction, *Proc Natl Acad Sci U S A 90*, 3710-3714.
13. Chelly, J., and Desguerre, I. (2013) Progressive muscular dystrophies, *Handbook of clinical neurology 113*, 1343-1366.
14. Koenig, M., Beggs, A. H., Moyer, M., Scherpf, S., Heindrich, K., Bettecken, T., Meng, G., Muller, C. R., Lindlof, M., Kaariainen, H., and et al. (1989) The molecular basis for Duchenne versus Becker muscular dystrophy: correlation of severity with type of deletion, *Am J Hum Genet 45*, 498-506.
15. Gardner, K. L., Kearney, J. A., Edwards, J. D., and Rafael-Fortney, J. A. (2006) Restoration of all dystrophin protein interactions by functional domains in trans does not rescue dystrophy, *Gene Ther 13*, 744-751.
16. Warner, L. E., DelloRusso, C., Crawford, R. W., Rybakova, I. N., Patel, J. R., Ervasti, J. M., and Chamberlain, J. S. (2002) Expression of Dp260 in muscle tethers the actin cytoskeleton to the dystrophin-glycoprotein complex and partially prevents dystrophy, *Hum Mol Genet 11*, 1095-1105.

17. Love, D. R., Hill, D. F., Dickson, G., Spurr, N. K., Byth, B. C., Marsden, R. F., Walsh, F. S., Edwards, Y. H., and Davies, K. E. (1989) An autosomal transcript in skeletal muscle with homology to dystrophin, *Nature 339*, 55-58.
18. Khurana, T. S., Hoffman, E. P., and Kunkel, L. M. (1990) Identification of a chromosome 6-encoded dystrophin-related protein, *The Journal of biological chemistry 265*, 16717-16720.
19. Khurana, T. S., Watkins, S. C., Chafey, P., Chelly, J., Tome, F. M., Fardeau, M., Kaplan, J. C., and Kunkel, L. M. (1991) Immunolocalization and developmental expression of dystrophin related protein in skeletal muscle, *Neuromuscul Disord 1*, 185-194.
20. Belanto, J. J., Mader, T. L., Eckhoff, M. D., Strandjord, D. M., Banks, G. B., Gardner, M. K., Lowe, D. A., and Ervasti, J. M. (2014) Microtubule binding distinguishes dystrophin from utrophin, *Proceedings of the National Academy of Sciences of the United States of America 111*, 5723-5728.
21. Li, D., Bareja, A., Judge, L., Yue, Y., Lai, Y., Fairclough, R., Davies, K. E., Chamberlain, J. S., and Duan, D. (2010) Sarcolemmal nNOS anchoring reveals a qualitative difference between dystrophin and utrophin, *Journal of cell science 123*, 2008-2013.
22. Tinsley, J., Deconinck, N., Fisher, R., Kahn, D., Phelps, S., Gillis, J. M., and Davies, K. (1998) Expression of full-length utrophin prevents muscular dystrophy in mdx mice, *Nat Med 4*, 1441-1444.
23. Mendell, J. R., Campbell, K., Rodino-Klapac, L., Sahenk, Z., Shilling, C., Lewis, S., Bowles, D., Gray, S., Li, C., Galloway, G., Malik, V., Coley, B., Clark, K. R., Li, J., Xiao, X., Samulski, J., McPhee, S. W., Samulski, R. J., and Walker, C. M. (2010) Dystrophin immunity in Duchenne's muscular dystrophy, *N Engl J Med 363*, 1429-1437.
24. Mendell, J. R., Rodino-Klapac, L., Sahenk, Z., Malik, V., Kaspar, B. K., Walker, C. M., and Clark, K. R. (2012) Gene therapy for muscular dystrophy: lessons learned and path forward, *Neurosci Lett 527*, 90-99.
25. Partridge, T. A. (2011) Impending therapies for Duchenne muscular dystrophy, *Curr Opin Neurol 24*, 415-422.
26. Moxley, R. T., 3rd, Pandya, S., Ciafaloni, E., Fox, D. J., and Campbell, K. (2010) Change in natural history of Duchenne muscular dystrophy with long-term corticosteroid treatment: implications for management, *J Child Neurol 25*, 1116-1129.
27. Bushby, K., Finkel, R., Birnkrant, D. J., Case, L. E., Clemens, P. R., Cripe, L., Kaul, A., Kinnett, K., McDonald, C., Pandya, S., Poysky, J., Shapiro, F., Tomezsko, J., and Constantin, C. (2010) Diagnosis and management of Duchenne muscular dystrophy, part 1: diagnosis, and pharmacological and psychosocial management, *Lancet Neurol 9*, 77-93.
28. Bushby, K., Finkel, R., Birnkrant, D. J., Case, L. E., Clemens, P. R., Cripe, L., Kaul, A., Kinnett, K., McDonald, C., Pandya, S., Poysky, J., Shapiro, F., Tomezsko, J., and Constantin, C. (2010) Diagnosis and management of Duchenne

muscular dystrophy, part 2: implementation of multidisciplinary care, *Lancet Neurol 9*, 177-189.
29. Manzur, A. Y., Kuntzer, T., Pike, M., and Swan, A. (2008) Glucocorticoid corticosteroids for Duchenne muscular dystrophy, *Cochrane Database Syst Rev*, CD003725.
30. Ruegg, U. T. (2013) Pharmacological prospects in the treatment of Duchenne muscular dystrophy, *Current opinion in neurology 26*, 577-584.
31. Lai, Y., and Duan, D. (2012) Progress in gene therapy of dystrophic heart disease, *Gene therapy 19*, 678-685.
32. England, S. B., Nicholson, L. V., Johnson, M. A., Forrest, S. M., Love, D. R., Zubrzycka-Gaarn, E. E., Bulman, D. E., Harris, J. B., and Davies, K. E. (1990) Very mild muscular dystrophy associated with the deletion of 46% of dystrophin, *Nature 343*, 180-182.
33. Koo, T., Okada, T., Athanasopoulos, T., Foster, H., Takeda, S., and Dickson, G. (2011) Long-term functional adeno-associated virus-microdystrophin expression in the dystrophic CXMDj dog, *J Gene Med 13*, 497-506.
34. Kaplan, J. M., Kim, S. H., North, K. N., Rennke, H., Correia, L. A., Tong, H. Q., Mathis, B. J., Rodriguez-Perez, J. C., Allen, P. G., Beggs, A. H., and Pollak, M. R. (2000) Mutations in ACTN4, encoding alpha-actinin-4, cause familial focal segmental glomerulosclerosis, *Nature genetics 24*, 251-256.
35. Lee, S. H., Weins, A., Hayes, D. B., Pollak, M. R., and Dominguez, R. (2008) Crystal structure of the actin-binding domain of alpha-actinin-4 Lys255Glu mutant implicated in focal segmental glomerulosclerosis, *J Mol Biol 376*, 317-324.
36. Weins, A., Schlondorff, J. S., Nakamura, F., Denker, B. M., Hartwig, J. H., Stossel, T. P., and Pollak, M. R. (2007) Disease-associated mutant alpha-actinin-4 reveals a mechanism for regulating its F-actin-binding affinity, *Proceedings of the National Academy of Sciences of the United States of America 104*, 16080-16085.
37. Hunter, S., Jones, P., Mitchell, A., Apweiler, R., Attwood, T. K., Bateman, A., Bernard, T., Binns, D., Bork, P., Burge, S., de Castro, E., Coggill, P., Corbett, M., Das, U., Daugherty, L., Duquenne, L., Finn, R. D., Fraser, M., Gough, J., Haft, D., Hulo, N., Kahn, D., Kelly, E., Letunic, I., Lonsdale, D., Lopez, R., Madera, M., Maslen, J., McAnulla, C., McDowall, J., McMenamin, C., Mi, H., Mutowo-Muellenet, P., Mulder, N., Natale, D., Orengo, C., Pesseat, S., Punta, M., Quinn, A. F., Rivoire, C., Sangrador-Vegas, A., Selengut, J. D., Sigrist, C. J., Scheremetjew, M., Tate, J., Thimmajanarthanan, M., Thomas, P. D., Wu, C. H., Yeats, C., and Yong, S. Y. (2012) InterPro in 2011: new developments in the family and domain prediction database, *Nucleic Acids Res 40*, D306-312.
38. Koenig, M., Monaco, A. P., and Kunkel, L. M. (1988) The complete sequence of dystrophin predicts a rod-shaped cytoskeletal protein, *Cell 53*, 219-228.
39. Gimona, M., Djinovic-Carugo, K., Kranewitter, W. J., and Winder, S. J. (2002) Functional plasticity of CH domains, *FEBS Lett 513*, 98-106.
40. Rybakova, I. N., Amann, K. J., and Ervasti, J. M. (1996) A new model for the interaction of dystrophin with F-actin, *J Cell Biol 135*, 661-672.

41. Rybakova, I. N., and Ervasti, J. M. (2005) Identification of spectrin-like repeats required for high affinity utrophin-actin interaction, *J Biol Chem 280*, 23018-23023.
42. Rybakova, I. N., Patel, J. R., Davies, K. E., Yurchenco, P. D., and Ervasti, J. M. (2002) Utrophin binds laterally along actin filaments and can couple costameric actin with sarcolemma when overexpressed in dystrophin-deficient muscle, *Mol Biol Cell 13*, 1512-1521.
43. Way, M., Pope, B., Cross, R. A., Kendrick-Jones, J., and Weeds, A. G. (1992) Expression of the N-terminal domain of dystrophin in E. coli and demonstration of binding to F-actin, *FEBS Lett 301*, 243-245.
44. Moores, C. A., and Kendrick-Jones, J. (2000) Biochemical characterisation of the actin-binding properties of utrophin, *Cell motility and the cytoskeleton 46*, 116-128.
45. Norwood, F. L., Sutherland-Smith, A. J., Keep, N. H., and Kendrick-Jones, J. (2000) The structure of the N-terminal actin-binding domain of human dystrophin and how mutations in this domain may cause Duchenne or Becker muscular dystrophy, *Structure 8*, 481-491.
46. Keep, N. H., Winder, S. J., Moores, C. A., Walke, S., Norwood, F. L., and Kendrick-Jones, J. (1999) Crystal structure of the actin-binding region of utrophin reveals a head-to-tail dimer, *Structure 7*, 1539-1546.
47. Borrego-Diaz, E., Kerff, F., Lee, S. H., Ferron, F., Li, Y., and Dominguez, R. (2006) Crystal structure of the actin-binding domain of alpha-actinin 1: evaluating two competing actin-binding models, *J Struct Biol 155*, 230-238.
48. Franzot, G., Sjoblom, B., Gautel, M., and Djinovic Carugo, K. (2005) The crystal structure of the actin binding domain from alpha-actinin in its closed conformation: structural insight into phospholipid regulation of alpha-actinin, *J Mol Biol 348*, 151-165.
49. Sevcik, J., Urbanikova, L., Kost'an, J., Janda, L., and Wiche, G. (2004) Actin-binding domain of mouse plectin. Crystal structure and binding to vimentin, *Eur J Biochem 271*, 1873-1884.
50. Klein, M. G., Shi, W., Ramagopal, U., Tseng, Y., Wirtz, D., Kovar, D. R., Staiger, C. J., and Almo, S. C. (2004) Structure of the actin crosslinking core of fimbrin, *Structure 12*, 999-1013.
51. Galkin, V. E., Orlova, A., VanLoock, M. S., Rybakova, I. N., Ervasti, J. M., and Egelman, E. H. (2002) The utrophin actin-binding domain binds F-actin in two different modes: implications for the spectrin superfamily of proteins, *J Cell Biol 157*, 243-251.
52. Sutherland-Smith, A. J., Moores, C. A., Norwood, F. L., Hatch, V., Craig, R., Kendrick-Jones, J., and Lehman, W. (2003) An atomic model for actin binding by the CH domains and spectrin-repeat modules of utrophin and dystrophin, *J Mol Biol 329*, 15-33.
53. Lin, A. Y., Prochniewicz, E., James, Z. M., Svensson, B., and Thomas, D. D. (2011) Large-scale opening of utrophin's tandem calponin homology (CH)

domains upon actin binding by an induced-fit mechanism, *Proc Natl Acad Sci U S A 108*, 12729-12733.
54. Klare, J. P., and Steinhoff, H. J. (2009) Spin labeling EPR, *Photosynth Res 102*, 377-390.
55. de Vera, I. M., Blackburn, M. E., Galiano, L., and Fanucci, G. E. (2013) Pulsed EPR Distance Measurements in Soluble Proteins by Site-Directed Spin Labeling (SDSL), *Curr Protoc Protein Sci 74*, 17 17 11-17 17 29.
56. Jeschke, G., and Polyhach, Y. (2007) Distance measurements on spin-labelled biomacromolecules by pulsed electron paramagnetic resonance, *Phys Chem Chem Phys 9*, 1895-1910.
57. Reginsson, G. W., and Schiemann, O. (2011) Pulsed electron-electron double resonance: beyond nanometre distance measurements on biomacromolecules, *The Biochemical journal 434*, 353-363.
58. Madasu, Y., Suarez, C., Kast, D. J., Kovar, D. R., and Dominguez, R. (2013) Rickettsia Sca2 has evolved formin-like activity through a different molecular mechanism, *Proceedings of the National Academy of Sciences of the United States of America 110*, E2677-2686.
59. Prochniewicz, E., Zhang, Q., Janmey, P. A., and Thomas, D. D. (1996) Cooperativity in F-actin: binding of gelsolin at the barbed end affects structure and dynamics of the whole filament, *J Mol Biol 260*, 756-766.
60. Jeschke, G., Chechik, V., Ionita, P., Godt, A., Zimmermann, H., Banham, J., Timmel, C. R., Hilger, D., and Jung, H. (2006) DeerAnalysis2006—a comprehensive software package for analyzing pulsed ELDOR data, *Appl. Magn. Reson. 30*, 473-498.
61. Thompson, L. V., Lowe, D. A., Ferrington, D. A., and Thomas, D. D. (2001) Electron paramagnetic resonance: a high-resolution tool for muscle physiology, *Exerc Sport Sci Rev 29*, 3-6.
62. Brunger, A. T., Strop, P., Vrljic, M., Chu, S., and Weninger, K. R. (2011) Three-dimensional molecular modeling with single molecule FRET, *J Struct Biol 173*, 497-505.
63. Arai, Y., and Nagai, T. (2013) Extensive use of FRET in biological imaging, *Microscopy (Oxf) 62*, 419-428.
64. Percy, A. J., Rey, M., Burns, K. M., and Schriemer, D. C. (2012) Probing protein interactions with hydrogen/deuterium exchange and mass spectrometry-a review, *Anal Chim Acta 721*, 7-21.
65. Gupta, S., Celestre, R., Petzold, C. J., Chance, M. R., and Ralston, C. (2014) Development of a microsecond X-ray protein footprinting facility at the Advanced Light Source, *J Synchrotron Radiat 21*, 690-699.
66. Cavanagh, J. (2007) *Protein NMR spectroscopy : principles and practice*, 2nd ed., Academic Press, Amsterdam ; Boston.
67. Rule, G. S., and Hitchens, T. K. (2006) *Fundamentals of protein NMR spectrosopy*, Springer, Dordrecht.
68. Teng, Q. (2012) *Structural biology : practical NMR applications*, Springer, New York.

69. Wang, X., Lee, H. W., Liu, Y., and Prestegard, J. H. (2011) Structural NMR of protein oligomers using hybrid methods, *J Struct Biol 173*, 515-529.